Eur. Phys. J. Plus (2017) **132**: 412
DOI 10.1140/epjp/i2017-11667-5

THE EUROPEAN PHYSICAL JOURNAL PLUS

Regular Article

Numerical study of entropy generation in MHD water-based carbon nanotubes along an inclined permeable surface

Feroz Ahmed Soomro[1], Rizwan-ul-Haq[2,a], Z.H. Khan[3], and Qiang Zhang[1]

[1] Department of Mathematics, Nanjing University, Nanjing 210093, China
[2] Department of Electrical Engineering, Bahria University, Islamabad, Pakistan
[3] Department of Mathematics, University of Malakand, Dir (Lower), Khyber Pakhtunkhwa, Pakistan

Received: 15 July 2017 / Revised: 20 August 2017
Published online: 4 October 2017 –

Abstract. Main theme of the article is to examine the entropy generation analysis for the magneto-hydrodynamic mixed convection flow of water functionalized carbon nanotubes along an inclined stretching surface. Thermophysical properties of both particles and working fluid are incorporated in the system of governing partial differential equations. Rehabilitation of nonlinear system of equations is obtained via similarity transformations. Moreover, solutions of these equations are further utilized to determine the volumetric entropy and characteristic entropy generation. Solutions of governing boundary layer equations are obtained numerically using the finite difference method. Effects of two types of carbon nanotubes, namely, single-wall carbon nanotubes (SWCNTs) and multi-wall carbon nanotubes (MWCNTs) with water as base fluid have been analyzed over the physical quantities of interest, namely, surface skin friction, heat transfer rate and entropy generation coefficients. Influential results of velocities, temperature, entropy generation and isotherms are plotted against the emerging parameter, namely, nanoparticle fraction $0 \leq \phi \leq 0.2$, thermal convective parameter $0 \leq \lambda \leq 5$, Hartmann number $0 \leq M \leq 2$, suction/injection parameter $-1 \leq S \leq 1$, and Eckert number $0 \leq Ec \leq 2$. It is finally concluded that skin friction increases due to the increase in the magnetic parameter, suction/injection and nanoparticle volume fraction, whereas the Nusselt number shows an increasing trend due to the increase in the suction parameter, mixed convection parameter and nanoparticle volume fraction. Similarly, entropy generation shows an opposite behavior for the Hartmann number and mixed convection parameter for both single-wall and multi-wall carbon nanotubes.

1 Introduction

A nanofluid is a kind of fluid which is the composition of conventional fluids, such as water, oil, etc., and small-sized particles called nanoparticles of size less than 100 nm. Deep investigation of the literature shows that Choi and Eastman [1] were the first who gave the idea of combining a simple fluid with nanoparticles and named it a nanofluid. In contrast to a simple fluid, the nanofluid is found to have different thermophysical effects, such as viscosity, thermal conductivity, thermal diffusivity, etc. [2]. It is being used in numerous industrial fields, such as nuclear reactors, medicine, transportation, etc. For detailed study of nanofluid scope the readers are suggested to read [3]. After the introduction of nanofluids, many researchers started revisiting the problems studied before using simple fluids. Nanofluids have also earned a good position in the field of heat transfer problems. According to the scope of the present paper, we will not give reference to experimental studies but only to some recent numerical study of such problems. The study of flow and heat transfer of a nanofluid over a vertical stretching sheet was done by Dongonchi and Ganji [4]. Two types of nanoparticles, CuO and Al_2O_3 were incorporated in the water base fluid. Numerical solution of the problem was presented while considering buoyancy and radiation effects. Another study using single-wall and multi-wall carbon nanotubes combined with water was done to investigate the flow along streamwise and cross flow direction [5]. Two-dimensional stagnation-point nanofluid flow and heat transfer were taken into consideration by Freidoonimehr *et al.* [6] using the Buongiorno fluid model. A comparative study of four water-based nanofluids containing Ag, Cu, TiO_2 and Al_2O_3 nanoparticles, was done by Aly [7]. The existence of multiple solutions was reported using exact solution. Flow and heat transfer of a three-dimensional MHD nanofluid flow and heat transfer over nonlinear bidirectional stretching

[a] e-mail: ideal_riz@hotmail.com, r.haq.qau@gmail.com (corresponding author)

surface were studied by Mahanthesh *et al.* [8]. Again, water-based nanofluids containing Cu, Al_2O_3 and TiO_3 were used as the working fluid.

Mixed convection flow is a kind of flow where heat is transferred through both force convection and natural convection. In the field of boundary layer flow over stretching surfaces, the flow considered along the surface where gravity plays a role in free convection combined with the flow due to stretching of surface is a kind of mixed convection flow. Here we will discuss some recently reported results of mixed convection flow over an inclined stretching surface (with an angle of 90 degree, it will be a vertical surface). Two-dimensional boundary layer flow and heat transfer over an inclined stretching surface under the effects of magnetic and viscous dissipation were analyzed by Afridi *et al.* [9]. The inclined stretching sheet was considered as non-permeable, the prescribed surface temperature and numerical solution of the problem were obtained. The Oldroyd-B non-Newtonian fluid flow over an inclined stretching surface was studied by Ashraf *et al.* [10]. The problem focused on the thermal radiation effects on the flow and heat transfer characteristics. The problem was solved analytically using the homotopy analysis method. Apart from the mixed convection flow of simple fluids, much attention has also been paid to the nanofluid flow over inclined stretching surfaces. Bala and Reddy [11] studied the flow of a non-Newtonian Casson nanofluid over an inclined exponential stretching surface. The detailed study was done numerically considering velocity slip, thermal slip and Solutal slip. While studying the mixed convection flow of the nanofluid over the inclined stretching sheet, Dhani *et al.* [12] discovered multiple solutions for a certain range of physical parameters. The three-dimensional flow of a Maxwell nanofluid over an inclined stretching surface was studied by Ashraf *et al.* [13]. The effects of radiation and thermophoresis were analyzed on the flow and heat transfer characteristics of the nanofluid. The problem of Burgers' nanofluid flow over an inclined stretching sheet with heat and mass transfer was dealt with by Hayat *et al.* [14]. The solution was obtained analytically using the homotopy analysis method. Apart from the inclined surface, analyses have also been performed for horizontal flat surfaces discussed by various authors in the last years [15–25].

The concept of entropy generation is very crucial in the study of heat transfer problems. The entropy is the disorder which is generated in a physical system due to many irreversible processes, such as friction, electrical resistance, chemical reactions, etc. Since the system could not be brought to its initial state without utilizing extra energy, the main objective is to minimize the generation of entropy. The literature shows that Bejan [26] and Qing [27] were the first who calculated the entropy generation in the process of heat and fluid flow. Later on, many researchers have given close attention to this important factor in the heat transfer problems. Entropy generation analysis of the non-Newtonian Casson nanofluid flow over a stretching sheet was carried by Qing *et al.* [28]. In another study, Dalir *et al.* [29] considered the Jeffrey nanofluid flow over a stretching sheet and analyzed the entropy generation under the effects of magnetic field, Brownian motion and thermophoresis. The entropy generation of a viscoelastic MHD nanofluid flow over a stretching sheet was done by Sajjad *et al.* [30].

The purpose of this paper is to carry out a numerical study on the entropy generation of a two-dimensional MHD mixed convection nanofluid flow and heat transfer over an inclined stretching sheet. Two types of nanoparticles, namely single-wall and multi-wall carbon nanotubes, are used to make the working nanofluid, whereas water is used as the base fluid. The limiting case of our model with no suction and normal fluid (without nanoparticles) reduces to the one studied recently by Afridi *et al.* [9]. Formulation of the model is presented in mathematical framework (sect. 2). Then entropy generation analysis is defined in sect. 3. Comparison of the present study with the existing literature is validated and further results are computed in the methodology sect. 4. In sect. 5, a whole discussion of the present model against emerging parameters is carefully addressed. Comprehensive analysis is described in the form of conclusion in the last sect. 6.

2 Mathematical framework

Consider the 2D mixed convection nanofluid flow along permeable inclined stretching surface, which makes an angle of $\alpha = 45^\circ$ with respect to the horizontal axis. The surface is linearly stretching with velocity $u_w(x) = cx$, where c is an arbitrary constant. A uniform magnetic field, B_0, normal to the stretching surface is also applied. Under the considered assumptions and after applying necessary boundary layer approximations the Cartesian form of the governing equations may be written as (see fig. 1 for graphical representation)

$$\frac{\partial u}{\partial x} + \frac{\partial u}{\partial y} = 0, \tag{1}$$

$$u\frac{\partial u}{\partial x} + v\frac{\partial u}{\partial y} = \vartheta_{nf}\frac{\partial^2 u}{\partial y^2} + g\frac{(\rho\beta)_{nf}}{\rho_{nf}}(T - T_\infty)\cos\alpha - \frac{\sigma B_0^2}{\rho_{nf}}u, \tag{2}$$

$$u\frac{\partial T}{\partial x} + v\frac{\partial T}{\partial y} = \alpha^*_{nf}\frac{\partial^2 T}{\partial y^2} + \frac{\mu_{nf}}{(\rho C_p)_{nf}}\left(\frac{\partial u}{\partial y}\right)^2, \tag{3}$$

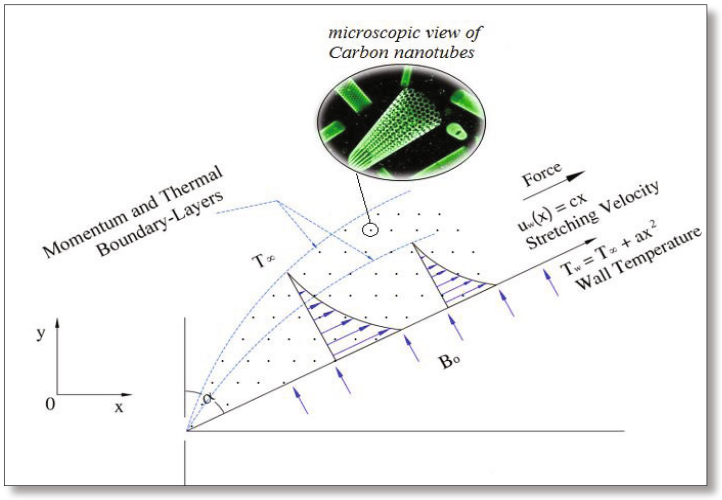

Fig. 1. Geometry of the model.

Table 1. Thermophysical properties of the base fluid and nanoparticles.

Physical properties	Base fluid (water)	Nanoparticles	
		SWCNTs	MWCNTs
ρ (kg/m^3)	997	2.600	1.600
C_p (J/kgK)	4.179	425	796
k (W/mK)	0.613	6.600	3.000
$\beta \times 10^5$ (K^{-1})	21	1.9	2.1
Pr	6.2		

where u and v are the respective velocities in the x- and y-directions, respectively, ϑ_{nf} is the kinematic viscosity of the nanofluid, g is the acceleration due to gravity, β_{nf} is the coefficient of thermal expansion of the nanofluid, ρ_{nf} is the density of the nanofluid, T and T_∞ are the fluid temperature and ambient fluid temperature, respectively, α is the angle of inclination between horizontal and stretching surfaces, α^*_{nf} is the thermal diffusivity of nanofluid, μ_{nf} is the thermal diffusivity of the nanofluid and $(C_p)_{nf}$ is the specific heat capacity of nanofluid. The above-mentioned parameters are defined as

$$\begin{aligned}
\vartheta_{nf} &= \frac{\mu_{nf}}{\rho_{nf}}, \qquad \mu_{nf} = \frac{\mu_f}{(1-\phi)^{2.5}}, \qquad \rho_{nf} = (1-\phi)\rho_f + \phi\rho_s,\\
(\rho\beta)_{nf} &= (1-\phi)(\rho\beta)_f + \phi(\rho\beta)_s, \qquad \alpha^*_{nf} = \frac{k_{nf}}{(\rho C_p)_{nf}},\\
k_{nf} &= k_f \left(\frac{1-\phi+2\phi\left(\frac{k_s}{k_s-k_f}\right)\ln\left(\frac{k_s+k_f}{2k_f}\right)}{1-\phi+2\phi\left(\frac{k_f}{k_s-k_f}\right)\ln\left(\frac{k_s+k_f}{2k_f}\right)} \right),\\
(\rho C_p)_{nf} &= (1-\phi)\,(\rho C_p)_f + \phi\,(\rho C_p)_s\,.
\end{aligned} \tag{4}$$

In the above relations, ϕ represents the nanoparticle fraction against the base fluid, subscript f and s represent the properties of base fluid and nanoparticles, respectively. The values of the base fluid and nanoparticles are given in table 1. Moreover, we consider the temperature at the stretching surface T_w of the form $T_w = T_\infty + ax^2$, where a is an arbitrary constant. Then the corresponding boundary conditions for eqs. (1)–(3) are set as

$$\begin{aligned}
&u = u_w(x), \quad v = v_w(y), \quad T = T_w(x) \quad \text{at } y = 0,\\
&u \to 0, \quad T \to 0 \quad \text{as } y \to \infty,
\end{aligned} \tag{5}$$

where v_w is the mass transfer velocity across the permeable stretching surface, which will be defined later. To non-dimensionalize the above governing equations, we introduce the following similarity transformations:

$$\psi = (c\vartheta_f)^{1/2} x f(\eta), \qquad \theta(\eta) = \frac{T - T_\infty}{T_w - T_\infty}, \qquad \eta = \sqrt{\frac{c}{\vartheta_f}}\, y, \tag{6}$$

where the stream function ψ is defined as $u = \partial\psi/\partial y$ and $v = -\partial\psi/\partial x$. Using (6) it can be verified easily that the continuity equation (1) is identically satisfied and eqs. (2) and (3) along with boundary conditions (5) take the following non-linear differential equations form:

$$\frac{1}{(1-\phi)^{2.5}\left(1-\phi+\frac{\rho_s}{\rho_f}\phi\right)} f'''(\eta) + f(\eta) f''(\eta) - (f'(\eta))^2 + \frac{\left(1-\phi+\frac{(\rho\beta)_s}{(\rho\beta)_f}\phi\right)\lambda\cos\alpha}{\left(1-\phi+\frac{\rho_s}{\rho_f}\phi\right)}\theta(\eta) - \frac{M}{\left(1-\phi+\frac{\rho_s}{\rho_f}\phi\right)} f'(\eta) = 0, \tag{7}$$

$$\frac{\left(\frac{1-\phi+2\phi\left(\frac{k_s}{k_s-k_f}\right)\ln\left(\frac{k_s+k_f}{2k_f}\right)}{1-\phi+2\phi\left(\frac{k_f}{k_s-k_f}\right)\ln\left(\frac{k_s+k_f}{2k_f}\right)}\right)}{\left(1-\phi+\frac{(\rho C_p)_s}{(\rho C_p)_f}\phi\right)\mathrm{Pr}}\theta''(\eta) - 2f'(\eta)\theta(\eta) + f(\eta)\theta'(\eta) + \frac{Ec}{(1-\phi)^{2.5}\left(1-\phi+\frac{(\rho C_p)_s}{(\rho C_p)_f}\phi\right)}(f''(\eta))^2 = 0, \tag{8}$$

$$f(0) = S, \qquad f'(0) = 1, \qquad f'(\infty) = 0,$$
$$\theta(0) = 1, \qquad \theta(\infty) = 0, \tag{9}$$

where prime indicates differentiation with respect to independent similarity variable η, $\lambda = \frac{g\beta_f(T_w - T_\infty)x}{u_w^2}$ is the thermal convective parameter, $\mathrm{Pr} = \frac{\vartheta_f}{\alpha_f^*}$ is the Prandtl number, $Ec = \frac{u_w^2}{C_p(T_w - T_\infty)}$ is the Eckert number and $S = -\frac{v_w}{\sqrt{c\vartheta_f}}$ is the suction parameter. Skin friction coefficient C_f and Nusselt number Nu are defined as

$$C_f = \frac{\tau_w}{\rho_{nf} u_w^2}, \qquad Nu = \frac{x q_w}{\alpha_{nf}(T_w - T_\infty)}, \tag{10}$$

where τ_w and q_w are the stress tensor and heat flux, respectively. In dimensionless form, the skin friction coefficient and the Nusselt number are written as

$$\mathrm{Re}_x^{1/2} C_f = \frac{f''(0)}{(1-\phi)^{2.5}}, \qquad \mathrm{Re}_x^{-1/2} Nu = -\left(\frac{k_{nf}}{k_f}\right)\theta'(0). \tag{11}$$

3 Entropy generation analysis

The volumetric entropy generation for the considered problem is written as

$$S'''_{gen} = \frac{k_{nf}}{T_\infty^2}\left(\frac{\partial T}{\partial y}\right)^2 + \frac{\mu_{nf}}{T_\infty}\left(\frac{\partial u}{\partial y}\right)^2 + \frac{\sigma B_0^2}{T_\infty} u^2. \tag{12}$$

The entropy generation number is defined as the volumetric entropy generation rate, which is the ratio between generation rate and the characteristic entropy generation, and is defined as

$$Ns = \frac{S'''_{gen}}{S'''_0} = \mathrm{Re}\left\{\frac{k_{nf}}{k_f}(\theta'(\eta))^2 + \frac{1}{(1-\phi)^{2.5}}\frac{Br}{\Omega}\left(f''^2(\eta) + M^2 f'^2(\eta)\right)\right\}, \tag{13}$$

where S'''_0 is the characteristic entropy generation, Br is the Brinkman number, Ω is the non-dimensionless temperature difference parameter and M is the Hartmann number, whose expressions are given by

$$S'''_0 = \frac{k_f c}{\vartheta_f}, \qquad \mathrm{Re} = \frac{u_w(x)}{\vartheta_f}, \qquad Br = \frac{\mu_f u_w^2}{k_f(T_w - T_\infty)}, \qquad \Omega = \frac{T_w - T_\infty}{T_\infty}. \tag{14}$$

The Bejan number is defined as the ratio of the entropy generation due to heat transfer with the entropy generation due to viscous dissipation and magnetic effects and is defined as

$$Be = \frac{\frac{k_{nf}}{T_\infty^2}\left(\frac{\partial T}{\partial y}\right)^2}{\frac{\mu_{nf}}{T_\infty}\left(\frac{\partial u}{\partial y}\right)^2 + \frac{\sigma B_0^2}{T_\infty}u^2}. \tag{15}$$

In dimensionless form the Bejan number is written as

$$Be = \frac{\frac{k_{nf}}{k_f}\,\mathrm{Re}\,\theta'^2(\eta)}{\frac{\mathrm{Re}}{(1-\phi)^{2.5}}\left(\frac{Br}{\Omega}f''^2(\eta)+\frac{BrM^2}{\Omega}f'^2(\eta)\right)}. \tag{16}$$

4 Numerical procedure

For the purpose of brevity we may write eqs. (7)–(9) in the following form:

$$\frac{1}{\phi_1\phi_2}f'''(\eta)+f(\eta)f''(\eta)-\left(f'(\eta)\right)^2+\frac{\phi_3\lambda\cos\alpha}{\phi_2}\theta(\eta)-\frac{M}{\phi_2}f'(\eta)=0, \tag{17}$$

$$\frac{\phi_4}{\mathrm{Pr}\,\phi_5}\theta''(\eta)-2f'(\eta)\theta(\eta)+f(\eta)\theta'(\eta)+\frac{Ec}{\phi_1\phi_5}\left(f''(\eta)\right)^2=0, \tag{18}$$

$$f(0)=S,\qquad f'(0)=1,\qquad f'(\infty)=0,$$
$$\theta(0)=1,\qquad \theta(\infty)=0, \tag{19}$$

where

$$A_1=(1-\phi)^{2.5},$$
$$A_2=1-\phi+\frac{\rho_s}{\rho_f}\phi,$$
$$A_3=1-\phi+\frac{(\rho\beta)_s}{(\rho\beta)_f}\phi,$$
$$A_4=\left(\frac{1-\phi+2\phi\left(\frac{k_s}{k_s-k_f}\right)\ln\left(\frac{k_s+k_f}{2k_f}\right)}{1-\phi+2\phi\left(\frac{k_f}{k_s-k_f}\right)\ln\left(\frac{k_s+k_f}{2k_f}\right)}\right),$$
$$A_5=1-\phi+\frac{(\rho C_p)_s}{(\rho C_p)_f}\phi. \tag{20}$$

Let us define the auxiliary variables,

$$x_1=f,\qquad x_2=f',\qquad x_3=f',\qquad x_4=\theta,\qquad x_5=\theta'. \tag{21}$$

Then eqs. (17)–(19) take the following discretized form:

$$x_1'=x_2,$$
$$x_2'=x_3,$$
$$x_3'=A_1A_2\left(-x_1x_3+x_2^2\right)-A_1A_3\lambda\cos\alpha x_4+A_1Mx_2,$$
$$x_4'=x_5,$$
$$x_5'=\frac{\mathrm{Pr}\,A_5}{A_4}\left(2x_2x_4-x_1x_5\right)-\frac{\mathrm{Pr}\,Ec}{A_1A_4}x_3^2, \tag{22}$$

with the corresponding boundary conditions

$$x_1(\eta=0)=f(0)=S,$$
$$x_2(\eta=0)=f'(0)=1,$$
$$x_2(\eta\to\infty)=f'(\infty)=0,$$
$$x_4(\eta=0)=\theta(0)=1,$$
$$x_4(\eta\to\infty)=\theta(\infty)=0. \tag{23}$$

The above-discretized eqs. (22) and (23) are solved using the finite difference method. The uniform step size of 10^{-4} and truncation error tolerance of 10^{-8} is used. Using the infinity test it is concluded to restrict the infinite domain to $\eta=[0,12]$ to show the convergence of the obtained solution.

Table 2. Comparison of results in limiting case when $\phi = 0.0$ and $S = 0.0$.

	$\mathrm{Re}_x^{1/2} C_f$		$\mathrm{Re}_x^{-1/2} Nu_x$	
	Present	[9]	Present	[9]
λ	$\alpha = \pi/4$, $M = 1.0$, $\mathrm{Pr} = 0.7$, $Ec = 1.0$, $S = 0.0$			
0.0	−1.4142	−1.4142	0.5546	0.5546
0.5	−1.2427	−1.2427	0.6976	0.6976
1.0	−1.0886	−1.0886	0.7931	0.7931
1.5	−0.9439	−0.9439	0.8974	0.8974
M	$\lambda = 0.5$, $\alpha = \pi/4$, $\mathrm{Pr} = 0.7$, $Ec = 1.0$, $S = 0.0$			
0.0	−0.8155	−0.8155	0.9293	0.9293
0.5	−0.9359	−0.9359	0.8659	0.8659
1.0	−1.2427	−1.2427	0.6976	0.6976
1.5	−1.6479	−1.6479	0.4685	0.4685
Pr	$\lambda = 0.2$, $\alpha = \pi/4$, $M = 1.0$, $Ec = 1.0$, $S = 0.0$			
0.3	−1.3284	−1.3284	0.3897	0.3897
0.7	−1.3424	−1.3424	0.6219	0.6219
1.2	−1.3516	−1.3516	0.8106	0.8106
1.5	−1.3552	−1.3552	0.8962	0.8962
Ec	$\lambda = 0.2$, $\alpha = \pi/4$, $M = 1.0$, $\mathrm{Pr} = 1.2$, $S = 0.0$			
0.0	−1.3603	−1.3603	1.3873	1.3873

5 Results and discussion

5.1 Comparison

The system of eqs. (22) along with boundary conditions (23) were solved using the finite difference method. To show the validity of the obtained solutions we have shown a comparison of the present results with the already published ones, in the limiting case by not considering nanofluid and suction effects. A good agreement of the present results with the existing literature can be seen from table 2.

5.2 Variation of velocity and temperature profiles

Figures 2 and 3 show the profiles of velocity and temperature distribution of the nanofluid under the effects of emerging physical parameters for SWCNTs. It can be seen, from figs. 2(a)–(c), that the velocity of the nanofluid is always enhanced by increasing the nanoparticle volume fraction. Moreover, the velocity boundary layer thickness also increases due to the increase in the nanoparticle volume fraction. It can also be noted that the velocity of the nanofluid increases due to the increasing value of the thermal convection parameter and, conversely, decreases due to the increasing value of magnetic and suction parameters. On the other hand, it is evident, from figs. 3(a)–(c) that the temperature of the nanofluid decreases due to the increasing value of the thermal convection parameter and, conversely, increases due to the increasing value of magnetic and suction parameters. Again, the temperature of the nanofluid is also enhanced due to the increase in the nanoparticle volume fraction, as shown in figs. 3(a)–(c).

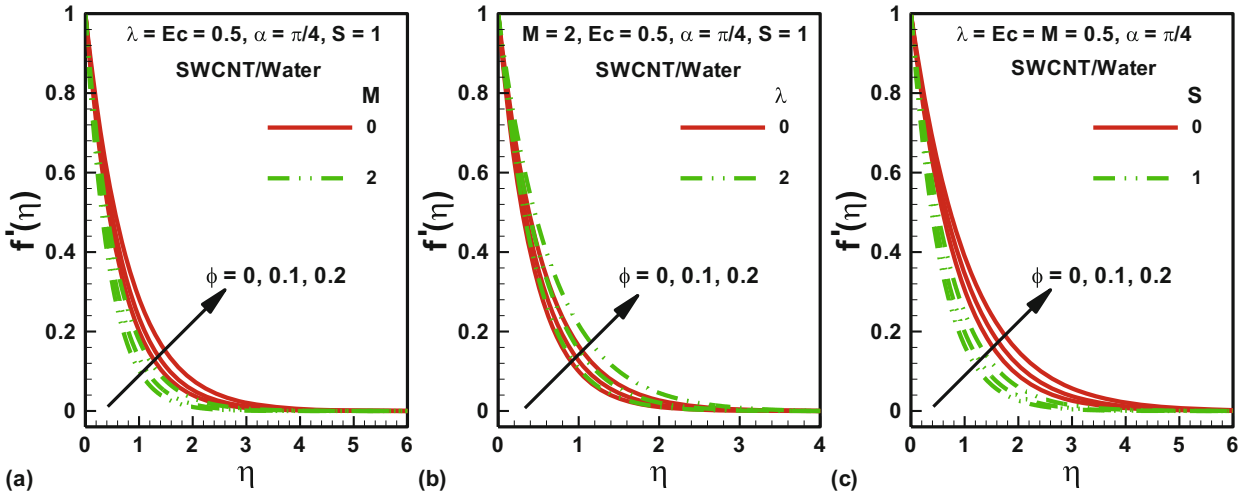

Fig. 2. Velocity profiles under the effects of various physical parameters.

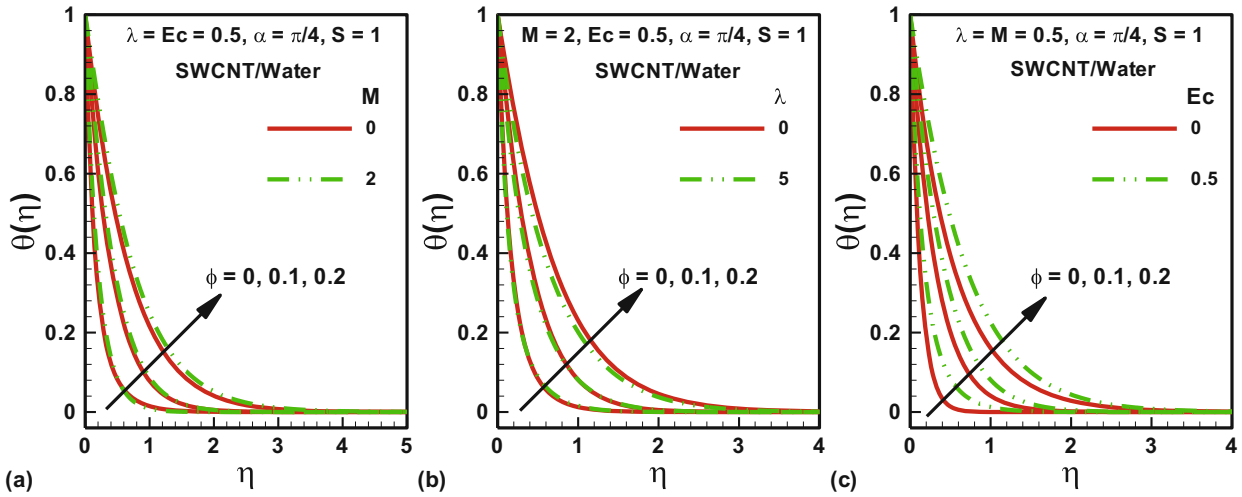

Fig. 3. Temperature profiles under the effects of various physical parameters.

5.3 Variation of skin friction and Nusselt number

Skin friction coefficient is also significantly affected by the emerging physical parameters. The graphs for both SWCNTs and MWCNTs against the magnetic parameter, mixed convection parameter, Eckert number and suction parameter are shown in figs. 4 and 5. It can be clearly noted that skin friction always tends to increase due to increase in the nanoparticle volume fraction for both SWCNTs and MWCNTs; however the skin friction is less for MWCNTs as compared to SWCNTs. Moreover, figs. 4(a) and 5(b) show that increasing the magnetic parameter produces an increase in the skin friction. On the other hand, an increase in the Eckert number and mixed convection parameter produces a decrease in skin friction which can be seen from figs. 4(b) and 5(a).

Due to the increase in the suction parameter and in the mixed convection parameter, the Nusselt number tends to increase whereas it tends to decrease due to increasing values of the magnetic parameter and Eckert number, which is shown in figs. 6 and 7. Overall, the Nusselt number tends to increase due to an increase in the nanoparticle volume fraction except in fig. 7(b), where for small values of the Eckert number, the Nusselt number tends to increase, but as the value of the Eckert number increases, the Nusselt number reverses its behavior, that is, it tends to decrease with increasing values of the nanoparticle volume fraction. Moreover, the Nusselt number for single-wall carbon nanotubes is less than for multi-wall carbon nanotubes, for the suction case only. It can be seen from fig. 6(a) that when the value of the suction parameter is less than zero, that is, in the injection case, the Nusselt number for single-wall carbon nanotubes is greater than for multi-wall carbon nanotubes, in comparison with the suction case where the Nusselt number for single-wall carbon nanotubes is less than for multi-wall carbon nanotubes.

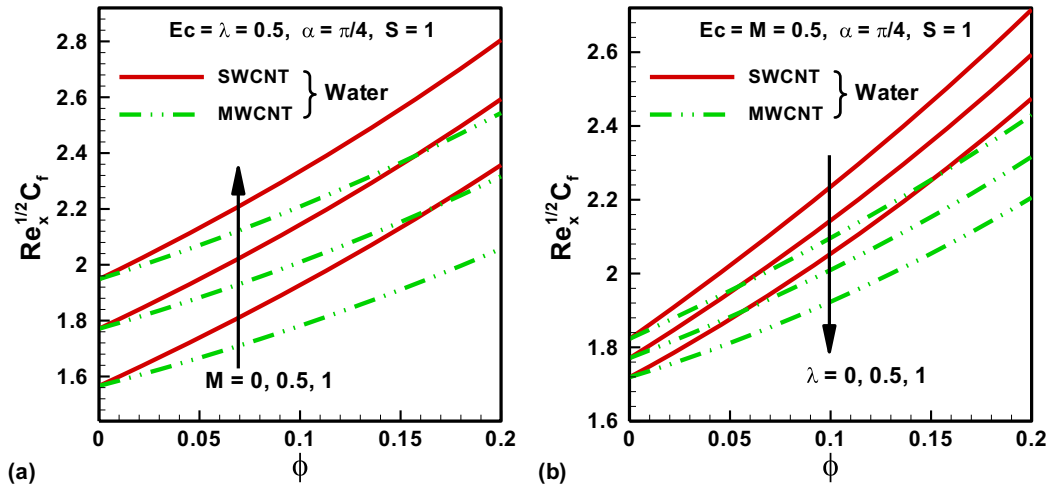

Fig. 4. Profiles of coefficient of skin friction under the effects of various physical parameters.

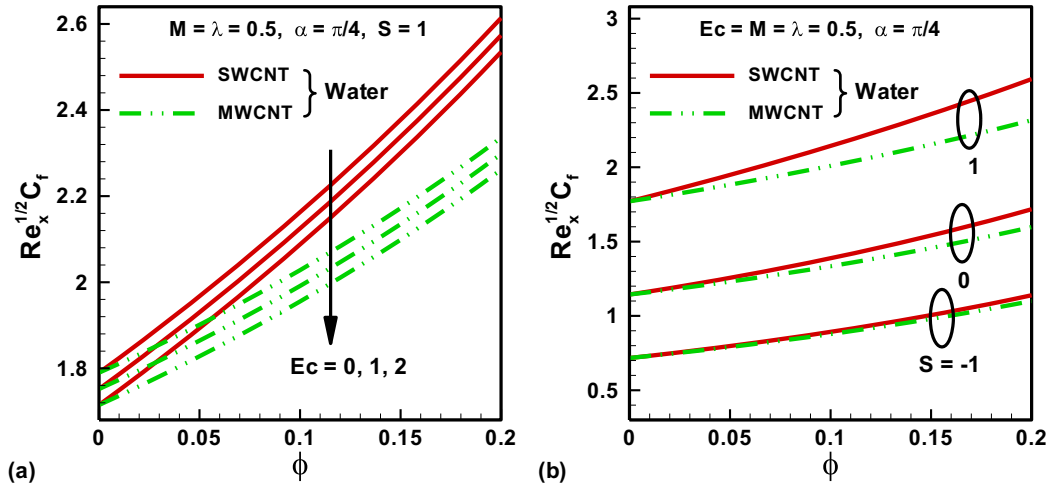

Fig. 5. Profiles of coefficient of skin friction under the effects of various physical parameters.

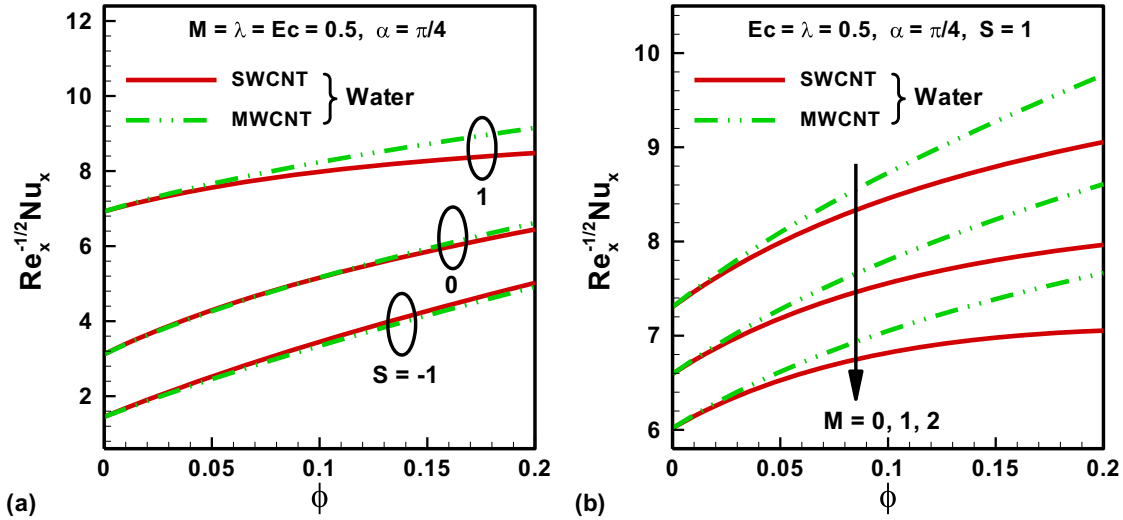

Fig. 6. Profiles of Nusselt number under the effects of various physical parameters.

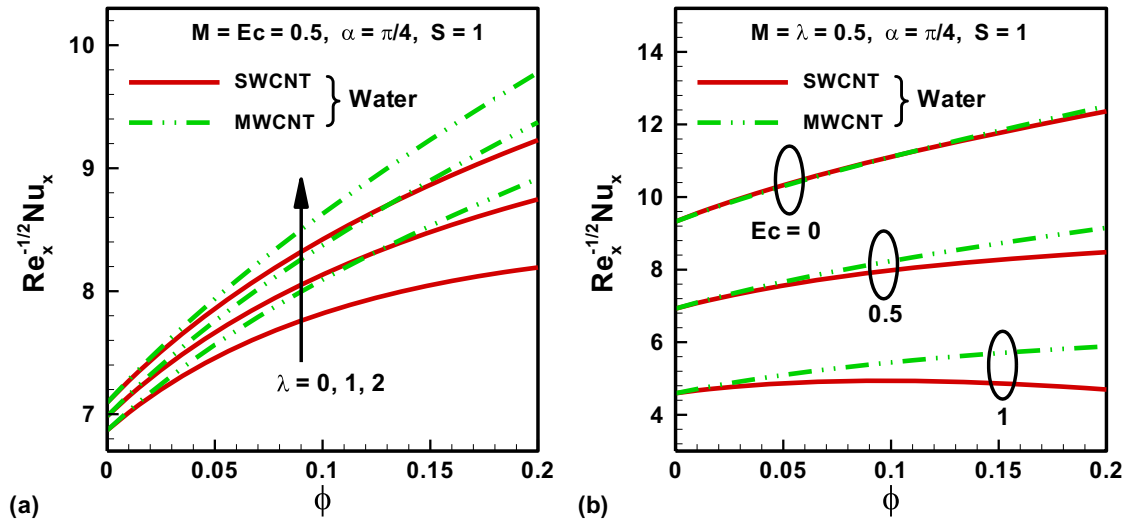

Fig. 7. Profiles of Nusselt number under the effects of various physical parameters.

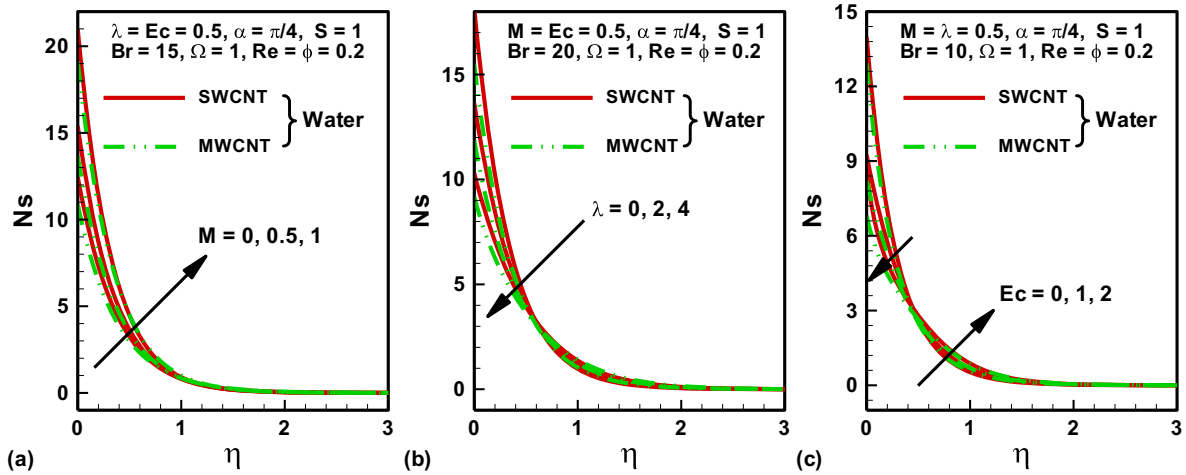

Fig. 8. Profiles of entropy generation under the effects of various physical parameters.

5.4 Variation of entropy generation number

Effects of physical parameters for both water-based single-wall and multi-wall carbon nanotubes on total entropy generation are shown in fig. 8. Overall, the entropy generation is less for multi-wall carbon nanotubes as compared to single-wall carbon nanotubes. Moreover, it is shown that the entropy generation number increases due to the increase in the magnetic parameter and, conversely, decreases due to the increase in the mixed convection parameter. Near the stretching surface the entropy generation has a decreasing effect due to the increase in the Eckert number, whereas away from the boundary layer it tends to a reverse behavior, that is, it increases due to the increase in the Eckert number. To further investigate the effects of the physical parameters on the entropy generation at the stretching sheet, see fig. 9. As can be observed in fig. 8, here it is also clear that for the nanoparticle volume fraction, the entropy generation tends to increase due to the increase in the magnetic parameter and to decrease due to the increase in mixed convection parameter and Eckert number. The nanoparticle volume fraction has different effects on the entropy generation at stretching sheet according to different combination of physical parameters. It is evident from fig. 9(a) that for small values of the magnetic parameter, the entropy generation decreases due to the increase in the nanoparticle volume fraction, but as the magnetic effects increase, the effects on the entropy generation is reversed, that is, for large values of the magnetic parameter the entropy generation increases due to the increase in the nanoparticle volume fraction. The same happens in the case of the Eckert number, where for comparatively small values of the Eckert number the entropy generation tends to decrease due to the increase in the nanoparticle volume fraction but, when large values of the Eckert number are considered, the entropy generation tends to increase due to the increase in the nanoparticle volume fraction.

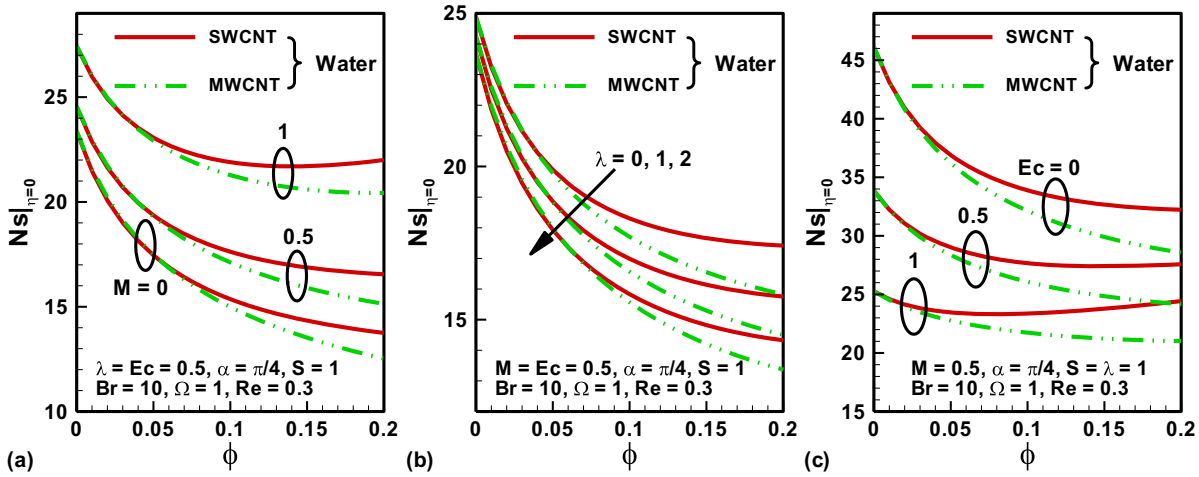

Fig. 9. Profiles of entropy generation at the stretching surface under the effects of physical parameters.

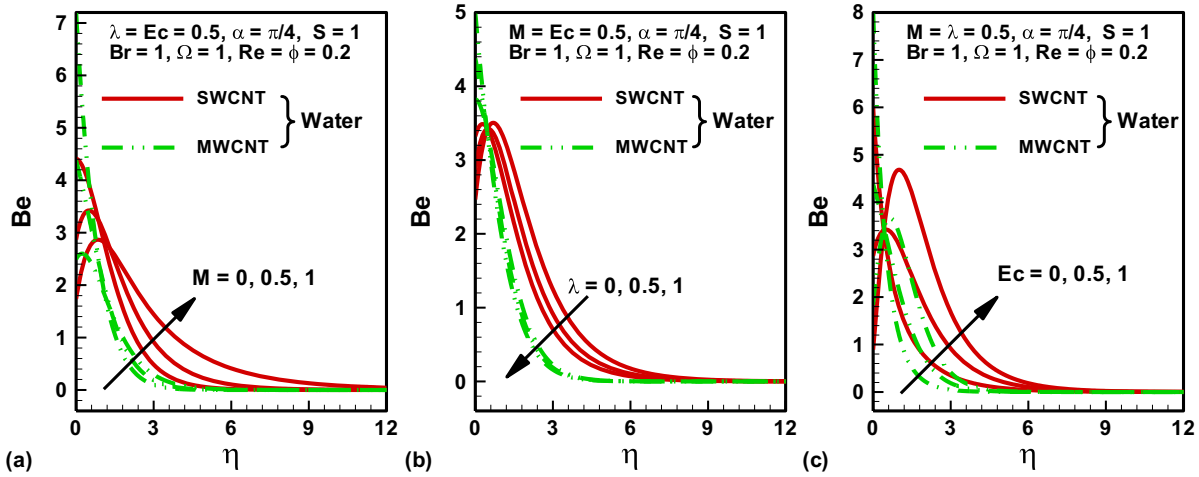

Fig. 10. Profiles of the Bejan number under the effects of various physical parameters.

5.5 Variation of Bejan number

Physical parameters have different effects on the Bejan number at the stretching surface and away from surface. The effects of contained parameters on the Bejan number away from the surface, but in the boundary layer region, may be seen from fig. 10. It is evident that using a nanofluid with single-wall and multi-wall carbon nanotubes, the Bejan number increases due to the increase in magnetic parameter and Eckert number, whereas an inverse behavior is observed due to the increase in the mixed convection parameter. This is the case for both single-wall and multi-wall carbon nanotubes. Moreover, it is observed that at the stretching sheet the physical parameters have opposite effects on the Bejan number, which is shown in fig. 11. It is clear that at the stretching surface the Bejan number tends to decrease due to the increase in the nanoparticle volume fraction for both single-wall and multi-wall carbon nanotubes; however, the Bejan number has a lower value for single-wall carbon nanotubes as compared to multi-wall carbon nanotubes. Moreover, the Bejan number increases due to the increase in the mixed convection parameter, whereas it decreases due to the increase in magnetic parameter and Eckert number. It is also observed that as the value of magnetic parameter and Eckert number the rate at which the Bejan number is decreased is also decreased significantly.

5.6 Variation of stream lines and isotherms

To detect the behavior of fluid molecules in the entire domain we have plotted the stream lines in fig. 12. These results are plotted for various values of the suction/injection parameter S. Similarly, the variation of temperature in the restricted domain of the model is plotted via isotherms (see fig. 13). Isotherms plots show a significant variation of temperature for various values of suction/injection parameter S.

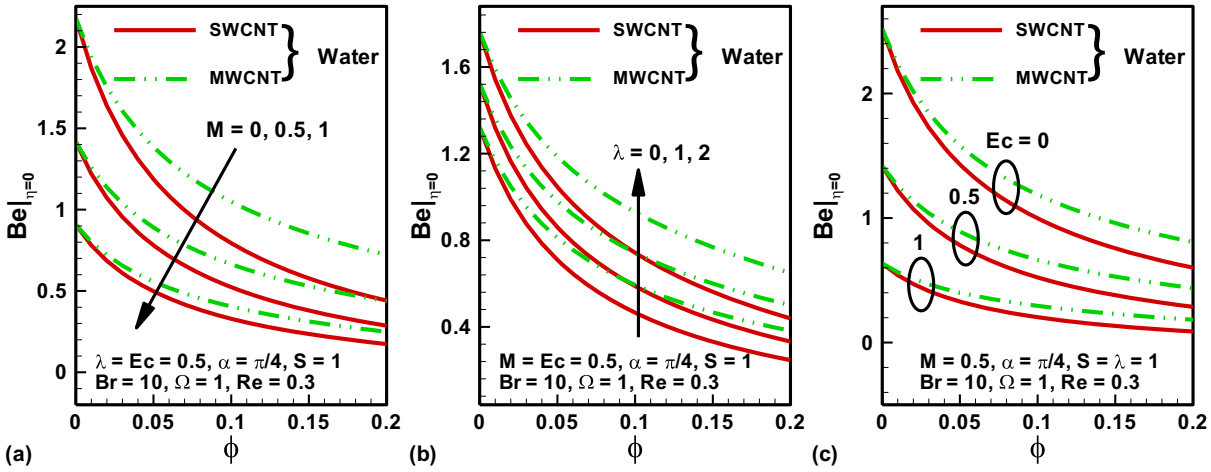

Fig. 11. Profiles of the Bejan number at the stretching surface under the effects of various physical parameters.

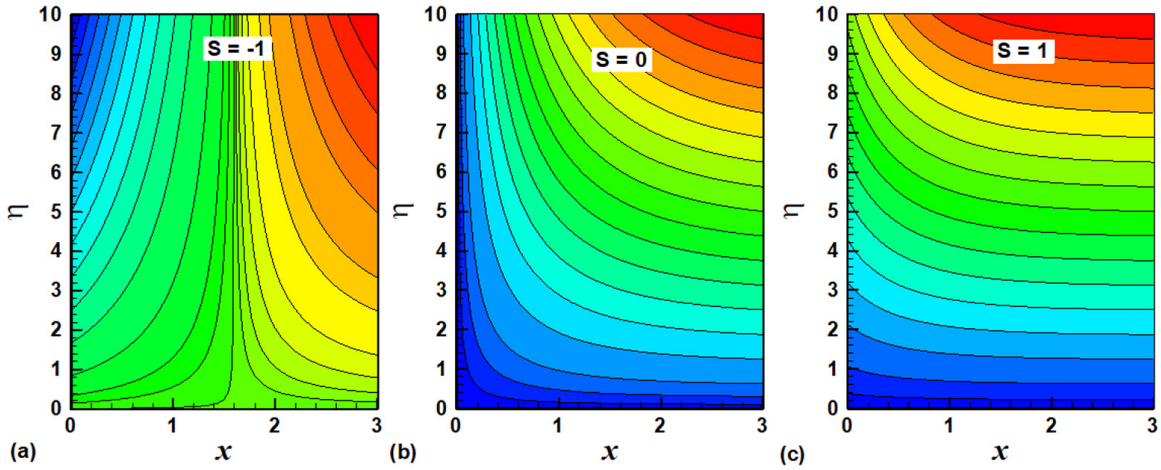

Fig. 12. Variation of stream lines for (a) $S = -1$ (b) $S = 0$ and (c) $S = 1$.

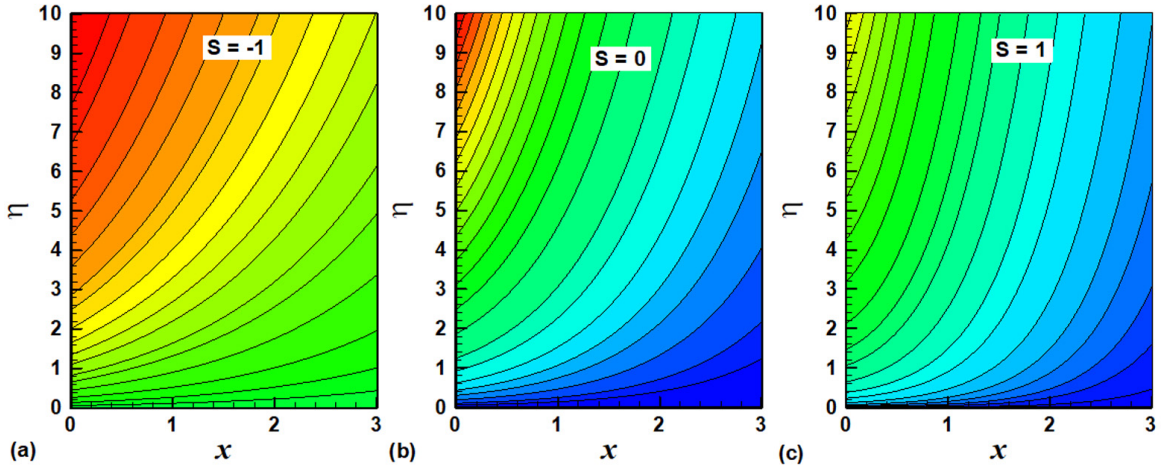

Fig. 13. Variation of isotherms for (a) $S = -1$, (b) $S = 0$ and (c) $S = 1$.

6 Conclusion

Entropy generation analysis for the two-dimensional mixed convection flow of a water-based nanofluid over an inclined stretching sheet with suction effect is performed numerically. Two types of nanoparticle, namely, single-wall carbon nanotubes and multi-wall carbon nanotubes, are used in this model. The system of governing partial differential equations is converted via similarity transformation into suitable nonlinear ordinary differential equations (ODEs). The finite difference method (FDM) is used to tackle ODEs in the computational software MatLab. Proper agreement of the results for the limiting case of the present model is shown via table 2 with the existing literature. The comprehensive key remarks on the performed study are the following:

- Velocity and temperature of the nanofluid are enhanced by increasing the volume of nanoparticles fraction. The velocity of the nanofluid decreases due to the increase in the magnetic and suction parameters whereas it increases due to the increase in the mixed convection parameter. For the same values an opposite trend is found for the temperature profile.
- Skin friction increases due to the increase in the Hartmann number, suction parameter and nanoparticle volume fraction, whereas a decreasing behavior is noted with an increase in mixed convection parameter and Eckert number.
- The Nusselt number shows increasing behavior due to the increase in the suction parameter, mixed convection parameter and nanoparticle volume fraction and it decreases due to the increase in the Hartmann and Eckert numbers.
- Entropy generation shows a decreasing behavior due to the Hartmann number and an increasing behavior due to the mixed convection parameter.
- Away from the surface but within the boundary layer region, the Bejan number increases due to the increase in magnetic parameter and Eckert number and it decreases due to the increase in the mixed convection parameter.

The first and last authors are thankful to the National Science Foundation of China (NSFC) for the financial support having grant number 11671199.

References

1. Stephen U.S. Choi, J.A. Eastman, *Enhancing thermal conductivity of fluids with nanoparticles*, presented at *ASME International Mechanical Engineering Congress and Exposition, 1995.*
2. Kiyuel Kwak, Chongyoup Kim, Korea-Australia Rheol. J. **17**, 35 (2005).
3. Kuafui V. Wong, Omar De Leon, Adv. Mech. Eng. **2010**, 519659 (2010).
4. Abdul Sattar Dogonchi, Davood Domiri Ganji, J. Mol. Liq. **223**, 521 (2016).
5. Riwan Ul Haq, Z.H. Khan, W.A. Khan, Inayat Ali Shah, Int. J. Chem. Reactor Eng. (2016) https://doi.org/10.1515/ijcre-2016-0059.
6. N. Freidoonimehr, M.M. Rashidi, B. Jalilpour, J. Braz. Soc. Mech. Sci. **38**, 1999 (2016).
7. Emad H. Aly, Powder Technol. **301**, 760 (2016).
8. B. Mahanthesh, B.J. Gireesha, R.S. Reddy Gorla, F.M. Abbasi, S.A. Shehzad, J. Magn. & Magn. Mater. **417**, 189 (2016).
9. Muhammad Idrees Afridi, Muhammad Qasim, Ilyas Khan, Sharidan Shafie, Ali Saleh Alshomrani, Entropy **19**, 10 (2017).
10. M. Bilal Ashraf, T. Hayat, A. Alsaedi, J. Appl. Mech. Tech. Phys. **57**, 317 (2016).
11. P. Bala Anki Reddy, Ain Shams Eng. J. **7**, 593 (2016).
12. Ruchika Dhanai, Puneet Rana, Lokendra Kumar, J. Taiwan Inst. Chem. Eng. **66**, 283 (2016).
13. M. Bilal Ashraf, T. Hayat, S.A. Shehzad, A. Alsaedi, AIP Adv. **5**, 027134 (2015).
14. T. Hayat, S. Asad, A. Alsaedi, J. Cent. South Univ. **22**, 3180 (2015).
15. Hashim, Masood Khan, Int. J. Heat Mass Transfer **103**, 291 (2016).
16. Hashim, M. Khan, J. Taiwan Inst. Chem. Eng. **77**, 282 (2017).
17. M. Khan, Hashim, Abdul Hafeez, Chem. Eng. Sci. https://doi.org/10.1016/j.ces.2017.07.024.
18. Hashim, M. Khan, Ali Saleh Alshomrani, J. Magn. & Magn. Mater. **443**, 13 (2017).
19. Hashim, M. Khan, Ali Saleh Alshomrani, Eur. Phys. J. E **40**, 8 (2017).
20. S. Nadeem, Rizwan Ul Haq, C. Lee, Sci. Iran. **19**, 1550 (2012).
21. N.S. Akbar, S. Nadeem, Rizwan Ul Haq, Z.H. Khan, Indian J. Phys. **87**, 1121 (2013).
22. S. Nadeem, Rizwan Ul Haq, Noreen Sher Akbar, Z.H. Khan, Alex. Eng. J. **52**, 577 (2013).
23. S. Nadeem, Rizwan Ul Haq, Z.H. Khan, J. Taiwan Inst. Chem. Eng. **45**, 121 (2014).
24. W.A. Khan, Z.H. Khan, Rizwan Ul Haq, Eur. Phys. J. Plus **130**, 86 (2015).
25. S.T. Hussain, S. Nadeem, Rizwan Ul Haq, Eur. Phys. J. Plus **129**, 167 (2014).
26. A. Bejan, Adv. Heat Transf. **15**, 1 (1982).
27. A. Bejan, *Entropy Generation Minimization: The Method of Thermodynamic Optimization of Finite-size Systems and Finite-time Processes* (CRC Press, Boca Raton, Fl, 1995).
28. J. Qing, M.M. Bhatti, M.A. Abbas, M.M. Rashidi, M. El-Sayed Ali, Entropy **18**, 123 (2016).
29. N. Dalir, M. Dehsara, S.S. Nourazar, Energy **79**, 351 (2015).
30. Sajjad-ur Rehman, Rizwan-ul Haq, Z.H. Khan, C. Lee, J. Taiwan Inst. Chem. Eng. **63**, 226 (2016).